

Article

Multimode Graded Index Fiber with Random Array of Bragg Gratings and Its Raman Lasing Properties

Alexey G. Kuznetsov ¹, Alexey A. Wolf ¹ , Zhibzema E. Munkueva ^{1,2}, Alexander V. Dostovalov ¹ and Sergey A. Babin ^{1,2,*}

¹ Institute of Automation and Electrometry SB RAS, 1 Acad. Koptyug Ave., 630090 Novosibirsk, Russia; kuznetsovag@iae.nsk.su (A.G.K.)

² Department of Physics, Novosibirsk State University, 1 Pirogova St., 630090 Novosibirsk, Russia

* Correspondence: babin@iae.nsk.su

Abstract: Light propagation in multimode fibers is known to experience various nonlinear effects, which are being actively studied. One of the interesting effects is the brightness enhancement at the Raman conversion of the multimode beam in graded index (GRIN) fiber due to beam cleanup at Raman amplification and mode selective feedback in the Raman laser cavity based on fiber Bragg gratings (FBGs) with special transverse structure. It is also possible to explore random distributed feedback based on Rayleigh backscattering on natural refractive index fluctuations in GRIN fibers, but it is rather weak, requiring very high power multimode pumping for random lasing. Here, we report on the first realization of femtosecond pulse-inscribed arrays of weak randomly spaced FBGs in GRIN fibers and study Raman lasing at its direct pumping by highly multimode ($M^2 \sim 34$) 940-nm laser diodes. The fabricated 1D–3D FBG arrays are used as a complex output mirror, together with the highly reflective input FBG in 1-km fiber. Above threshold pump power (~100 W), random lasing of the Stokes beam at 976 nm is obtained with output power exceeding 28 W at 174 W pumping. The beam quality parameter varies for different arrays, reaching $M^2 \sim 2$ at the linewidth narrowing to 0.1–0.2 nm due to the interference effects, with the best characteristics for the 2D array.



Citation: Kuznetsov, A.G.; Wolf, A.A.; Munkueva, Z.E.; Dostovalov, A.V.; Babin, S.A. Multimode Graded Index Fiber with Random Array of Bragg Gratings and Its Raman Lasing Properties. *Fibers* **2023**, *11*, 48. <https://doi.org/10.3390/fib11060048>

Academic Editor: Paulo Caldas

Received: 26 April 2023

Revised: 18 May 2023

Accepted: 19 May 2023

Published: 24 May 2023



Copyright: © 2023 by the authors. Licensee MDPI, Basel, Switzerland. This article is an open access article distributed under the terms and conditions of the Creative Commons Attribution (CC BY) license (<https://creativecommons.org/licenses/by/4.0/>).

1. Introduction

Nowadays, optical fibers are widely used in telecommunication, sensing and laser technologies due to their ability to efficiently generate, transmit and amplify optical signals, as well as to sense various environmental impacts precisely. Although single-mode fibers provide nearly one-dimensional (1D) light propagation along the fiber with a stable and robust transverse beam structure of the fundamental mode, they do not use transverse dimensions, thus limiting fiber transmission capacity. This is why multimode fibers have been actively studied in recent times in order to incorporate higher-order modes with a focus on the stability of multimode beam propagation in the presence of various linear and nonlinear effects of mode interaction [1–3].

One of key factors for signal attenuation in an optical fiber is the Rayleigh scattering of propagating light on random fluctuations of the refractive index at the sub-micron scale, which are naturally present in silica glass fibers. As some part of the scattered light is guided backwards in a fiber, Rayleigh backscattering (or reflection) is widely used as a sensing signal, and also as natural feedback in laser systems utilizing long fibers. So, random lasing in a cavity-free passive single-mode fiber is shown to be possible with single-mode pumping providing Raman gain and Rayleigh backscattering providing feedback, both distributed along the fiber [4]. Being actively studied during the last decade, random fiber lasers already outperform conventional single-mode fiber Raman lasers (with embedded FBG cavities for different Stokes orders) in terms of conversion efficiency at output powers

as high as ~ 1 kW [5] and tuning ranges reaching one octave (1–2 μm) when pumped by a Yb-doped fiber laser generating near 1 μm [6]. One interesting research possibility is to explore multimode passive fibers, which can be directly pumped by powerful, cheap and reliable multimode laser diodes (LDs). Cavities in multimode fibers may also be formed by in-fiber FBGs and/or random distributed feedback (RDFB) via Rayleigh backscattering.

The first experiments on multimode graded index (GRIN) fiber of 62.5 μm core with direct 940-nm LD pumping have shown that the natural Rayleigh backscattering in 4.5-km long GRIN fibers provides sufficient feedback, forming a half-open cavity with a highly reflective bulk mirror [7]. However, the obtained Raman lasing at 976 nm is less powerful and less stable than that with an output mirror instead of RDFB at this (see further, [8]) or other wavelengths (1020 nm) [9,10]. So, the next endeavors with multimode (MM) Raman fiber lasers (RFLs) were focused on LD-pumped RFLs with a linear cavity consisting of in-fiber reflectors instead of bulk mirrors, namely, multimode fiber Bragg gratings. As a result, the all-fiber scheme of such MM RFL with 915-nm LD-pumped 62.5- μm GRIN fiber has been demonstrated [11], which was then transferred to other LD wavelengths and MM core diameters (see [12] for a review). Impressive results have been achieved in generating relatively high power at short wavelengths (0.95–0.97 μm) [12] not available previously in either Yb-doped fiber laser (YDFL) or in YDFL-pumped conventional RFLs based on single-mode passive fibers with an FBG cavity [13]. An attractive feature of such LD-pumped Raman fiber lasers is the possibility to efficiently convert a highly multimode pump radiation into a Stokes beam, the quality of which turns out to be much better than that of the original pump beam, thanks to the Raman beam cleanup effect [14] and the additional transverse-mode selective feedback of the FBG cavity [12]. The use in the laser cavity of an output coupler based on FBG inscribed by femtosecond (fs) pulses in the near-axis area of the GRIN fiber core, corresponding to the fundamental mode, allows one to generate a near-diffraction-limited Stokes beam. So, in a linear cavity consisting of an FBG pair resonantly reflecting the Stokes beam at a wavelength of 976 nm during pumping by a multimode LD with beam quality $M^2 \approx 34$ at 940 nm, a high-quality ($M^2 \sim 2$) Stokes beam with output power of ~ 50 W has been obtained, thus demonstrating a record pump-to-Stokes brightness enhancement factor of 73 [15]. In [16,17], a two-stage cascaded Raman laser was demonstrated and the characteristics of the output radiation in the schemes with two FBG pairs for the first and second Stokes orders and the scheme with the half-open cavity based on random Rayleigh backscattering in the GRIN fiber itself (instead of output fs-inscribed FBG for the second order), were compared. It has been shown that in the case of Rayleigh scattering-based random distributed feedback, the efficiency of light conversion and the quality of the output second-order Stokes beam appear to be higher. The use of a natural random Rayleigh reflector in the second stage was possible due to the fact that the quality of the generated first-order Stokes beam was already quite high ($M^2 \sim 2$), and the second Stokes threshold was relatively easy to achieve at a relatively weak natural Rayleigh backscattering in a 1-km long GRIN fiber. For a random lasing of the first-order Stokes wave with low-quality pumping, a much longer GRIN fiber [7] or much higher pump power [18] is required. So, a random laser with ~ 300 W output power at 1120 nm has been achieved in a 120-m GRIN fiber at ~ 700 W multimode pumping by fiber-combined Yb-doped fiber lasers at 1070 nm [18]; however, the threshold pump power for such a Raman laser is as high as ~ 500 W. In [19], the threshold of random lasing in multimode LD-pumped GRIN fibers is reduced to ~ 140 W via enhanced backscattering on artificial fs-inscribed random structures, but rather low (~ 6 W) output power is achieved. To reduce the threshold and/or distributed cavity length of random lasers based on single-mode fibers, long Bragg gratings with randomized structures or arrays of short FBGs, randomly spaced along the fiber, have been implemented either in active fibers [20,21] or in passive fibers with Raman gain [22,23], resulting in narrowband random lasing in both cases. However, this approach has not yet been explored in multimode fibers.

Here, we study an opportunity to obtain low-threshold, high-power random Raman lasing in multimode LD-pumped GRIN fibers with the arrays of short fs-inscribed FBGs

with random structures either in longitudinal (1D) or in longitudinal plus one or two transverse directions (2D and 3D, respectively). The concrete array structure and the interference effects at beam reflection from individual FBGs influence both the spatial and spectral characteristics of the generated Stokes beam. The results of the 1D–3D FBG arrays' fabrication and characterization in the relationship with the Raman lasing properties of multimode GRIN fibers with in-fiber arrays are presented below.

2. Materials and Methods

The arrays of short ($L_{FBG} \leq 0.5$ mm) weakly reflective FBGs were inscribed in multimode GRIN fibers by a femtosecond point-by-point writing technique previously used for the inscription of ~1-cm long regular 1D FBGs [24], having been modified for writing 3D random structures. A beam of a mode-locked laser generating a train of 230-fs pulses at 1026 nm is focused by a 50X microscope objective with a high numerical aperture of $NA = 0.65$ (see Figure 1a). Each fs pulse changes the refractive index in the waist of the focused beam, thus forming a $\sim 1 \times 8 \mu\text{m}$ groove (with larger dimension along the beam) in the fiber core. The fiber translation along the z -axis at a constant speed of 0.658 mm/s at a fixed laser pulse repetition rate of 1 kHz results in the formation of grating with a period of $0.658 \mu\text{m}$ (FBG with the second order for a resonance reflection wavelength of 976.5 nm) (see Figure 1b). A high-precision air-bearing linear stage pulls the fiber through the glass ferrule with polished surfaces, which is placed on a 3D piezo stage in order to provide random shifts in the (x , y) plane at the z -translation. The transverse position of the individual FBG relative to the fiber axis was controlled by the visualization system based on two microscope objectives to view fiber displacements in x and y directions (see Figure 1a). For inscription of the 1D array with randomized positions of individual FBGs in the longitudinal direction, the transverse position of all FBGs was set by 3D piezo stage exactly on the fiber axis, whereas random longitudinal spacing between FBGs of length L_{FBG} was produced by an air-bearing linear stage with an average value of $\Delta L > L_{FBG}$, randomly varied within 20%. In case of 2D and 3D arrays, the axial shift is combined with random shifts (Δx , Δy) up to $\pm 5 \mu\text{m}$ off the axis in one (x) or two (x , y) transverse directions. A variety of FBG arrays (1D–3D) with different FBG lengths ($L_{FBG} = 0.5, 0.25$ mm), longitudinal FBG spacings ($\Delta L = 0.7, 0.33$ mm) and numbers of FBGs in the array ($N = 14, 28$), respectively, were inscribed, keeping nearly the same total reflection (around -15 dB) for the FBG arrays as that for regular fs-inscribed output FBG at 976 nm [15,25].

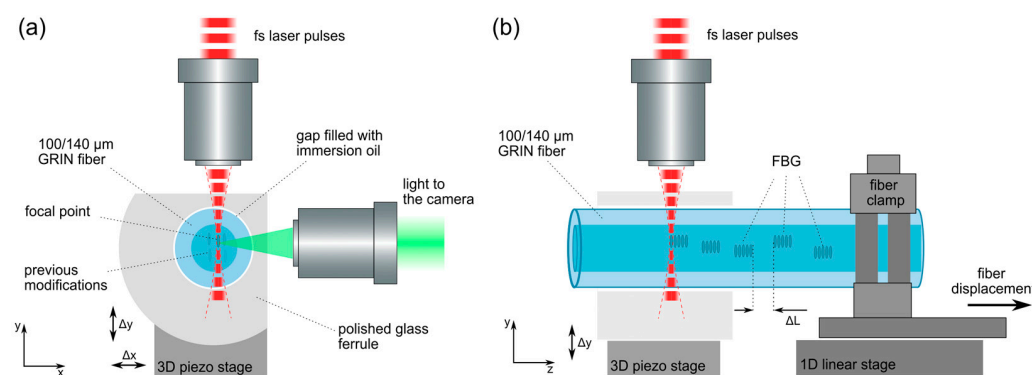


Figure 1. Scheme of writing weakly reflecting FBGs arrayed as 1D–3D structures: view along the fiber (a) and side view (b).

The corresponding reflection spectra for the fs-inscribed output random arrays of different types (1D, 2D, 3D), consisting of $N = 14$ FBGs, are shown in Figure 2b together with the reflection spectra of highly reflective UV-inscribed FBGs (which will be used as a highly reflective mirror of MM RFL cavity) in the 1D panel and 3D FBGs array with $N = 28$ in the 3D panel. The regular FBG has clear reflection peaks corresponding to different groups of transverse modes with ~ 0.4 nm spacing between them in 100- μm GRIN

core [12,24]. In the random FBG arrays, the interference of partially reflected light from individual FBGs in the random array leads to random irregularities in the spectrum with periods of $\sim 0.05\text{--}0.5$ nm so that the mode structure is washed out. Nevertheless, only a few (1–3) high-amplitude reflection peaks of random array overlap with the main peak of HR FBG centered at ~ 976.5 nm (corresponding to fundamental mode). The amplitudes of HR FBG peaks corresponding to higher order mode groups decrease from nearly -0.5 to about -10 dB for the fifth peak centered at 974.5 nm. A similar decrease of ~ 10 dB (from nearly -15 to -25 dB) is observed at the short wavelength tail of the random FBG array spectrum as its near-axis location leads to the predominant reflection of low-index modes. Since the shortest spectral period of the array is defined by its total length, and the longest period (~ 0.5 nm for array with $N = 14$) is defined by the spacing of neighboring FBGs, we also tested the array with $N = 28$ of short ($L_{FBG} \sim 0.25$ mm) FBGs, keeping the total array length nearly the same (~ 1.6 cm). For such a “dense” array, the longest period increases to ~ 1 nm; this is why its spectral characteristics become smoother and broader than those for $N = 14$, as illustrated in the 3D panel of Figure 2b.

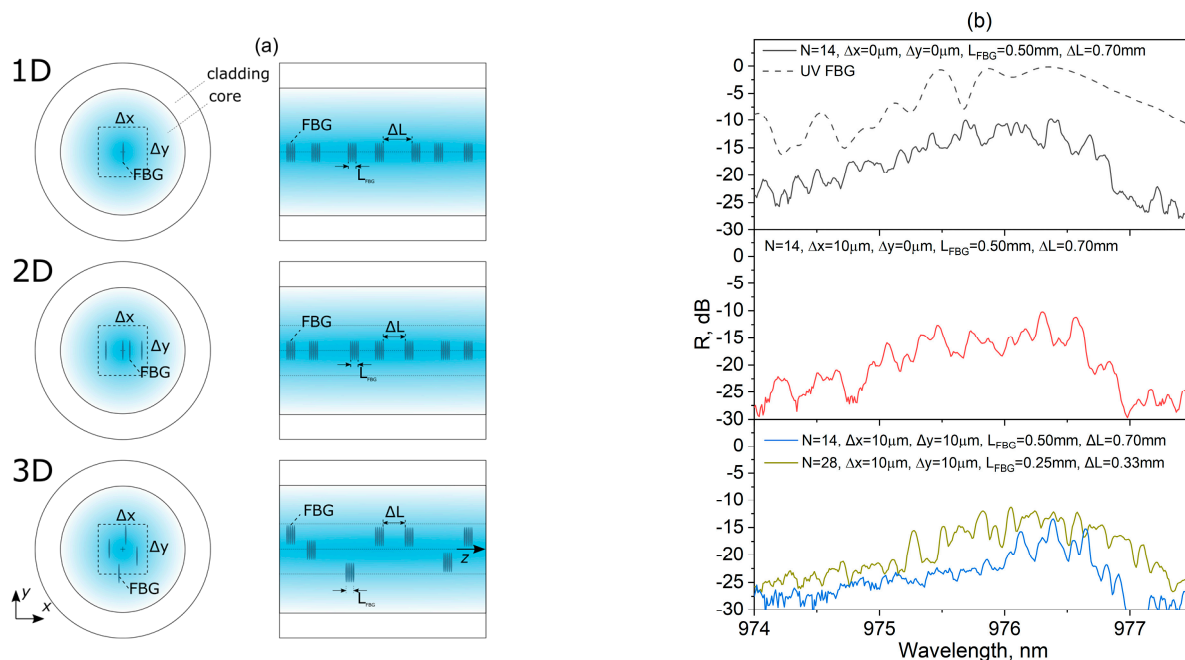


Figure 2. Random arrays of FBGs in GRIN fibers with $100/140\text{ }\mu\text{m}$ core/cladding: N parts of length L_{FBG} with average spacing ΔL along the z -axis (1D) plus transverse random shifts within Δx (2D) and Δx , Δy (3D) around the axis (a); and corresponding reflection spectra of the 1D–3D arrays of randomly spaced FBGs and UV FBG (b).

The fabricated random FBG arrays have been tested with a multimode fiber Raman laser whose scheme is shown in Figure 3. The pump radiation from three fiber-pigtailed high-power LDs operating at the wavelength of ~ 940 nm is added together by a 3×1 multimode fiber pump combiner. The input ports of the fused pump combiner are made of multimode step-index fiber with $105\text{-}\mu\text{m}$ core ($\text{NA} = 0.22$) because that in the LD pigtailed and the output port is made of the same GRIN fibers as that in Raman laser. The laser cavity consisted of a multimode GRIN fiber of $100/140\text{ }\mu\text{m}$ core/cladding diameter ($\text{NA} = 0.29$) with a length of 1 km and two reflectors at both ends. A highly reflective ($\sim 90\%$) FBG was spliced at the pump input, written by the phase mask technique with a UV laser at a first Stokes wavelength of 976 nm (its reflection spectrum is shown in Figure 2b, 1D panel). Instead of single regular 1D FBG, fs-inscribed along the axis of the GRIN fiber and used as output coupler in previous works [12,15,24,25], we have spliced at the output end a

random reflector consisting of N weakly reflecting FBGs arrayed as 1D, 2D or 3D structure (see Figure 2a), with characteristics shown in Figure 2b, 1D–3D panels.

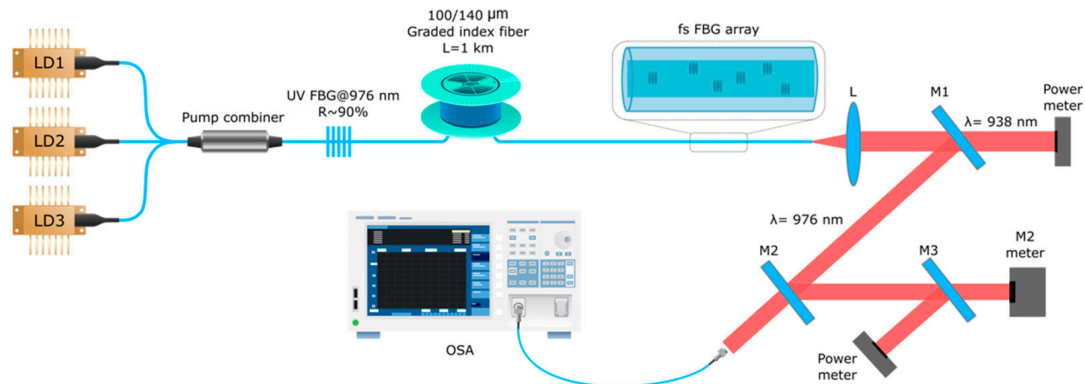


Figure 3. Scheme of a multimode Raman fiber laser: LD1–LD3—multimode laser diodes; UV FBG—high-reflective (HR) FBG inscribed using CW UV radiation; fs FBG array—fs-inscribed random FBG array, L—collimating lens; M1–M3—dichroic mirrors; OSA—optical spectrum analyzer.

3. Results

The output characteristics of the multimode LD-pumped RFL significantly vary for different random FBG arrays tested with the same HR FBG. The output power for the 1D–3D arrays with $N = 14$ and parameters demonstrated in Figure 2b are compared in Figure 4a. The threshold pump power for all of them is around ~ 100 W, whereas the output power measured at 174 W pumping amounts to 26, 28 and 18 W for the 1D, 2D and 3D arrays, respectively. In Figure 4b, we present the obtained values of output power as a function of the total reflection of the array, which significantly varies for different samples from $R \sim 1\%$ (-20 dB) to $R \sim 6\%$ (-12 dB). The overall tendency of power growth with increasing reflection and its saturation at $R \sim 4\%$ (similar to MM RFL with regular fs-inscribed output FBG [12,15]) can clearly be seen. At the same time, the 3D array provides maximum power at low R values (1–2%), whereas the 2D array gives the highest value at optimal R value ($\sim 4\%$) and the 1D array does it at the highest R value ($\sim 6\%$); these points (all with $N = 14$) are connected by solid line in Figure 4b.

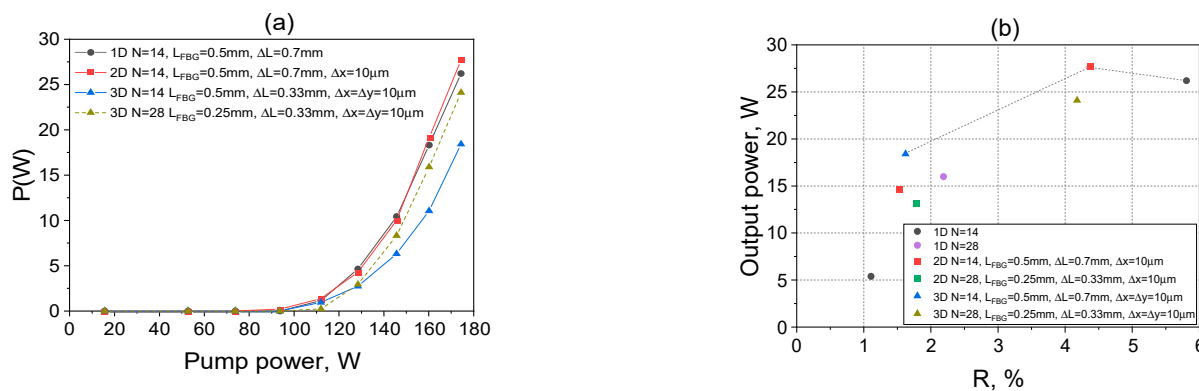


Figure 4. (a) Output power of MM RFL with arrays of $N = 14$ FBGs of different structure: black—1D ($L = 0.5$ mm, $\Delta L = 0.7$ mm); red—2D ($L = 0.5$ mm, $\Delta L = 0.7$ mm, $\Delta x = 10 \mu\text{m}$, $\Delta y = 0$); blue—3D ($L = 0.5$ mm, $\Delta L = 0.7$ mm, $\Delta x = \Delta y = 10 \mu\text{m}$); green— $N = 28$, 3D ($L = 0.25$ mm, $\Delta L = 0.33$ mm, $\Delta x = \Delta y = 10 \mu\text{m}$). (b) Output power at 174 W pumping for different 1D–3D FBG arrays versus their integral reflection at the generation wavelength near 976.5 nm (with averaging over generation spectrum).

It should be noted that it was difficult to obtain high R values for 2D arrays and especially for the 3D arrays with the same N , as their overlap with the fundamental mode is reduced. The increase of N from 14 to 28 at nearly the same length of the array does

not lead to a significant enhancement of power for 1D and 2D arrays (the power change nearly corresponds to relative change of R in 1–2% interval). For the 3D array, such a doubling of FBG number in the array leads to an increase of R to ~4%, providing, in turn, a corresponding increase of power to ~24 W (see Figure 4). However, it may additionally strengthen the role of higher order modes due to interference effects leading to a smooth reflection spectrum in large scale (>1 nm), thus enhancing its tail at <976 nm (see Figure 2b, 3D panel). So, it is also necessary to evaluate the generated mode composition based on the spatial analysis of the output beam.

In Figure 5, we present the data of beam quality and profile measurements obtained at the same generation power for 1D–3D random arrays with reflection spectra shown in Figure 2b. The 1D, 2D and 3D arrays with $N = 14$ (Figure 5a–c, respectively) show a rather good beam profile and quality parameter of $M^2 = 2.0\text{--}2.1$; at the same time, the 3D array provides sufficiently lower maximum power (see Figure 4a). The 3D array with $N = 28$ FBGs has a comparable maximum power to that of the 1D and 2D arrays (with $N = 14$) but a sufficiently worse beam quality, $M^2 \sim 2.7$ (see Figure 5d). This means that the power increase for the 3D array with $N = 28$ (in comparison to the 3D array with $N = 14$) occurs due to both the increase of integral reflection and the involvement of more higher-order mode groups in the generation leading to larger beam area.

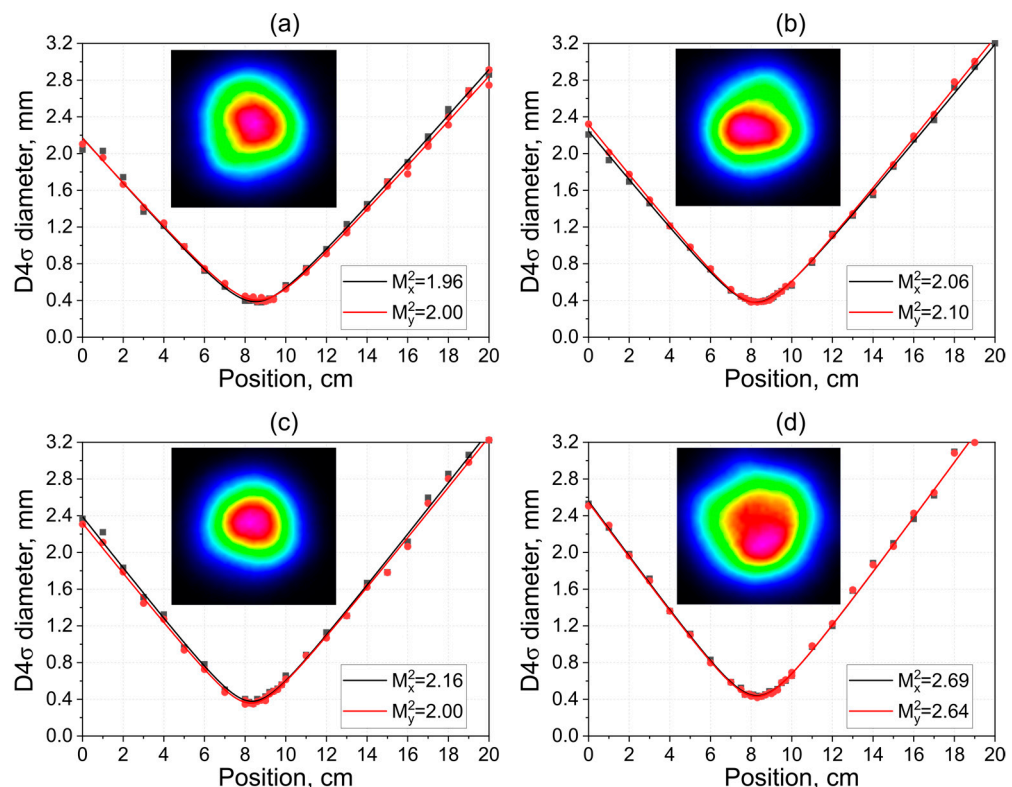


Figure 5. Beam profile and quality measurements of MM RFL at the same output power (~5 W) for different output reflectors: (a) 1D FBG array ($L = 0.5$ mm, $N = 14$, $\Delta L = 0.7$ mm), at increasing power parameter M^2 is measured to grow up to ~2.6. (b) 2D FBG array ($L = 0.5$ mm, $N = 14$, $\Delta L = 0.7$ mm, $\Delta x = 10$ μ m, $\Delta y = 0$). (c) 3D FBG array ($L = 0.5$ mm, $N = 14$, $\Delta L = 0.33$ mm, $\Delta x = \Delta y = 10$ μ m). (d) 3D FBG array ($L = 0.25$ mm, $N = 28$, $\Delta L = 0.33$ mm, $\Delta x = \Delta y = 10$ μ m).

A comparison of the laser spectra with the corresponding reflection spectra for 1D–3D FBG arrays with $N = 14$ (see Figure 2), generating high-quality beams of $M^2 \sim 2$, is presented in Figure 6a–c. One can see that the irregularities induced by the interference between the individual FBGs in the reflection spectra are reproduced somehow in the generation spectra; although, in all cases, the generation starts from a single peak, corresponding to maximum reflection, 1–3 neighbor reflection peaks also start to generate at higher powers

and then, at further power increases, they are washed out. In some cases, instabilities of the spectra (unstable spikes) appear at the short wavelength edge (see e.g., Figure 6a, 160 W pumping). For the 3D array with $N = 28$, which has the worst beam quality, the spectrum is not shown since it is the most unstable, especially in the short-wavelength tail corresponding to high-order modes. The high-power instabilities are less pronounced in the optimum case (2D array), and the main peak in the generation spectrum remains rather narrow with increasing power. In the case of the 2D array, we extract the -3 dB width of the generated line and present it in Figure 6d as a function of the output power. At low power, the linewidth is below 0.05 nm; then, it grows from ~ 0.1 nm to ~ 0.2 nm in power range $5\text{--}20$ W and exceeds 0.3 nm at the maximum power of 28 W, where the interference pattern is almost fully washed out by nonlinear spectral broadening. Nevertheless, the value is still lower than the linewidth of ~ 0.4 nm in MM RFL with regular FBG fs-inscribed in GRIN fibers [12,24,25], in which the interference effects are absent.

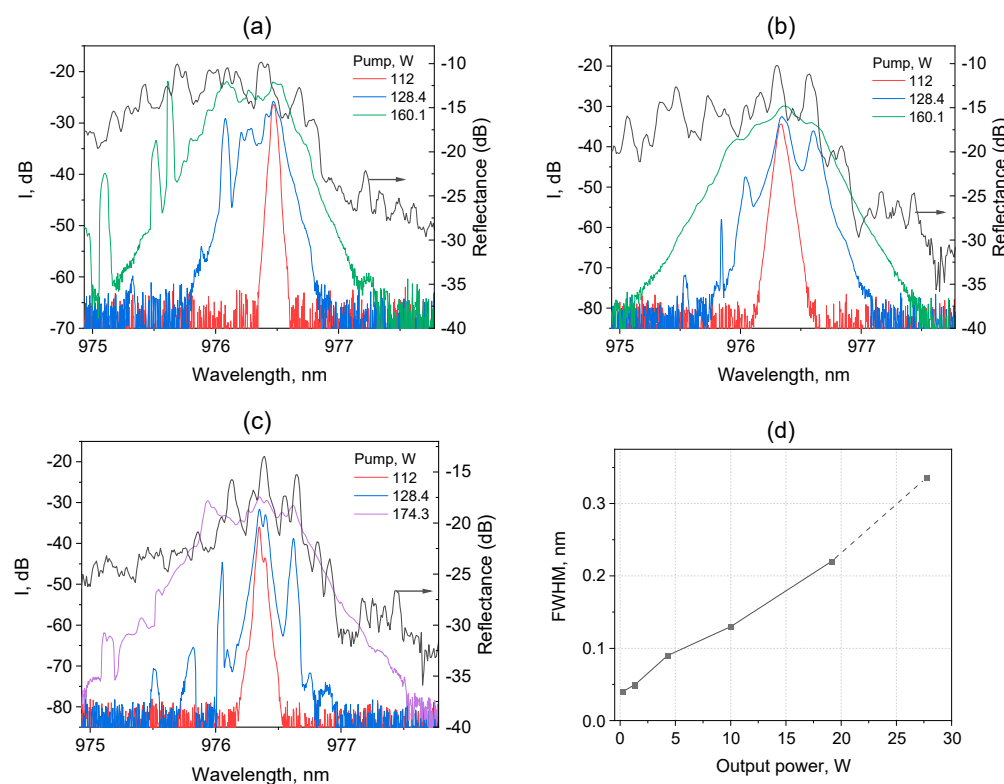


Figure 6. Output spectra of MM RFL at different pump powers in comparison with corresponding spectrum of FBG array ($N = 14$): (a) 1D ($L = 0.5$ mm, $N = 14$, $\Delta L = 0.7$ mm); (b) 2D ($L = 0.5$ mm, $N = 14$, $\Delta L = 0.7$ mm, $\Delta x = 10$ μ m, $\Delta y = 0$); (c) 3D ($L = 0.5$ mm, $N = 14$, $\Delta L = 0.5$ mm, $\Delta x = \Delta y = 10$ μ m); (d) -3 dB width (FWHM) of the generated Stokes line versus output power in the scheme with 2D FBG array.

4. Discussion and Conclusions

Thus, proof-of-principle experiments have been performed on the femtosecond inscription of random 1D–3D arrays of short $N = 14\text{--}28$ weakly reflecting FBGs in multimode GRIN fiber, which enable, together with the highly reflective FBG, a relatively low threshold (~ 100 W) of random Raman lasing at highly multimode ($M^2 \sim 34$ nm) laser diode pumping at 940 nm. The obtained output characteristics of the Stokes beam at 976 nm are shown to depend on the array structure. Similar to regular output FBG inscribed along the axis (1D) [15,25], the studied random arrays have optimal integral reflection of $\sim 4\%$, providing maximum output power of 28 W at 174 W pumping, obtained with a 2D reflector. Comparison of low-reflection (1–2%) arrays at the same pumping demonstrates maximum power (18 W) in the case of 3D array; whereas, for higher reflection ($\sim 6\%$), maximum power (26 W)

is obtained with the 1D array, all having $N = 14$ FBGs with $L_{FBG} \sim 0.5$ mm. The beam quality parameter M^2 , measured at moderate power, is close to 2 in all these cases. Increasing the FBG number to $N = 28$ does not significantly change power characteristics for 1D–2D arrays, and it enhances output power for 3D array (to 24 W at ~4% reflection), albeit at the expense of the beam quality worsening to $M^2 \sim 2.7$.

The analysis of the spatial and spectral characteristics of the generated Stokes beam in relationship with the reflection spectra of FBG arrays shows that the reflection spectrum for $N = 28$ is broader and smoother than that for $N = 14$ with the same total length. This is explained by the 2-times-broader spectral range of modulation periods (up to ~ 1 nm) induced by interference of partial reflections from individual FBGs in the array with 2-times-denser FBG packing. This effect leads to the increasing reflection of high-order modes at short wavelength tails and the corresponding beam quality worsening in the case of $N = 28$. The narrower spectral range of modulation periods (up to ~ 0.5 nm) for $N = 14$ FBGs leads to the better selection of fundamental mode for higher-order mode groups separated by ~ 0.4 nm. In addition, this also leads to the appearance of 0.1–0.3 nm interference patterns within the single-mode group that results in single-line generation with <0.1 nm linewidth near the threshold. Well above the threshold, 1–3 generated lines are broadened with increasing power, so that the overall generation spectrum remains narrowband (0.1–0.2 nm at –3 dB level) in the 5–20 W power range. At maximum power (~28 W), the interference-induced lines are washed out, and the integral spectrum broadens to >0.3 nm.

Thus, the random FBG arrays fs inscribed in multimode GRIN fibers enable output power and beam quality of the LD-pumped Raman laser comparable with that obtained earlier with the optimal fs-inscribed FBG of $R \sim 4\%$ at the wavelength of 976 nm [15,25]. At the same time, the generated spectrum is even narrower with random FBG array due to the interference effect leading to additional modulation of the reflection spectrum. Comparison of 1D–3D arrays shows that the best Raman laser characteristics are obtained with the 2D array, i.e., when longitudinal random shifts along the z -axis are combined with shifts off the axis in the transverse direction (x), which is perpendicular to the grating groove of $\sim 1 \times 8 \mu\text{m}$ size (in x and y directions, respectively). The random x -shift of the groove within $10 \mu\text{m}$ results in the nearly square structure of the 2D array in a transverse cross-section, which appears better for the predominant generation of the fundamental mode than the asymmetric strip-like or elliptical (with larger y -size) structures for 1D and 3D arrays, respectively. It is also interesting to fabricate FBG arrays with spiral structures that may help to generate, within the MM RFL cavity, the vortex modes or the beams containing a fractional topological charge [26].

In addition to the interesting physics of the nonlinear spatio-spectral transformation of the multimode Stokes beam at its interaction with the random array, this is a new technological approach, which enables a rather simple femtosecond pulse inscription of short, randomly spaced FBGs in the near-axis area of multimode fiber instead of a high-precision fabrication of long, on-axis FBGs. Such an all-fiber LD-pumped Raman laser also has good power scaling capabilities since the random FBG array is less sensitive to thermal load than the regular FBG; this is an important feature for practical applications. The applications also require a broader wavelength range availability. With commercially available high-power LDs operating at 915–976 nm, this approach may be easily extended from the presented 976 nm to the 950–1020 nm wavelength range as was already demonstrated for MM RFLs with regular RFLs [12,17], as well as to the 800–850 nm range with high power LD pumping at 790–800 nm. With the help of the second harmonic generation in nonlinear crystals, the MM RFL output beam of high quality ($M^2 \sim 2$ (first attempts are reported in [27])), can be efficiently converted into the visible range of 400–500 nm. Such lasers are in great demand for imaging/displays, as well as for Raman spectroscopy and microscopy, flow cytometry, high speed printing, holography, optical data storage and laser shows. The application range may be further extended by the next harmonics generation (e.g., to the UV range).

Author Contributions: Conceptualization, S.A.B.; methodology, A.A.W. and A.V.D.; validation, A.A.W. and Z.E.M.; investigation and data curation, A.A.W. and A.G.K.; writing—original draft preparation, A.G.K.; writing—review and editing, S.A.B.; funding acquisition, S.A.B. All authors have read and agreed to the published version of the manuscript.

Funding: This research was funded by Russian Science Foundation, grant 21-72-30024.

Data Availability Statement: Data underlying the results presented in this paper are not publicly available at this time but may be obtained from the authors upon reasonable request.

Acknowledgments: Experimental studies were carried out on the equipment of the Center for Collective Use “Spectroscopy and Optics” at the Institute of Automation and Electrometry SB RAS. The authors acknowledge the support of I. N. Nemov in the UV-laser inscription of HR FBG.

Conflicts of Interest: The authors declare no conflict of interest.

References

- Richardson, D.J.; Fini, J.M.; Nelson, L.E. Space-division multiplexing in optical fibres. *Nat. Photonics* **2013**, *7*, 354–362. [[CrossRef](#)]
- Wright, L.G.; Christodoulides, D.N.; Wise, F.W. Controllable spatiotemporal nonlinear effects in multimode fibres. *Nat. Photonics* **2015**, *9*, 306–310. [[CrossRef](#)]
- Krupa, K.; Tonello, A.; Shalaby, B.M.; Fabert, M.; Barthélémy, A.; Millot, G.; Wabnitz, S.; Couderc, V. Spatial beam self-cleaning in multimode fibres. *Nat. Photonics* **2017**, *11*, 234–241. [[CrossRef](#)]
- Turitsyn, S.K.; Babin, S.A.; El-Taher, A.E.; Harper, P.; Churkin, D.V.; Kablukov, S.I.; Ania-Castañón, J.D.; Karalekas, V.; Podivilov, E.V. Random distributed feedback fibre laser. *Nat. Photonics* **2010**, *4*, 231–235. [[CrossRef](#)]
- Zhang, H.; Wu, J.; Wan, Y.; Wang, P.; Yang, B.; Xi, X.; Wang, X.; Zhu, P. Kilowatt random Raman fiber laser with full-open cavity. *Opt. Lett.* **2022**, *47*, 493–496. [[CrossRef](#)] [[PubMed](#)]
- Zhang, L.; Jiang, H.; Yang, X.; Pan, W.; Cui, S.; Feng, Y. Nearly-octave wavelength tuning of a continuous wave fiber laser. *Sci. Rep.* **2017**, *7*, 42611. [[CrossRef](#)]
- Babin, S.A.; Dontsova, E.I.; Kablukov, S.I. Random fiber laser directly pumped by a high-power laser diode. *Opt. Lett.* **2013**, *38*, 3301–3303. [[CrossRef](#)] [[PubMed](#)]
- Kablukov, S.I.; Dontsova, E.I.; Zlobina, E.A.; Nemov, I.N.; Vlasov, A.A.; Babin, S.A. An LD-pumped Raman fiber laser operating below 1 μm. *Laser Phys. Lett.* **2013**, *10*, 085103. [[CrossRef](#)]
- Yao, T.; Harish, A.; Sahu, J.; Nilsson, J. High-power continuous-wave directly-diode-pumped fiber Raman lasers. *Appl. Sci.* **2015**, *5*, 1323–1336. [[CrossRef](#)]
- Glick, Y.; Fromzel, V.; Zhang, J.; Ter-Gabrielyan, N.; Dubinskii, M. High efficiency, 154 W CW, diode pumped Raman fiber laser with brightness enhancement. *Appl. Opt.* **2017**, *56*, B97–B102. [[CrossRef](#)]
- Zlobina, E.A.; Kablukov, S.I.; Wolf, A.A.; Nemov, I.N.; Dostovalov, A.V.; Tyrtyshnyy, V.A.; Myasnikov, D.V.; Babin, S.A. Generating high-quality beam in a multimode LD-pumped all-fiber Raman laser. *Opt. Express* **2017**, *25*, 12581–12587. [[CrossRef](#)] [[PubMed](#)]
- Babin, S.A.; Zlobina, E.A.; Kablukov, S.I. Multimode Fiber Raman Lasers Directly Pumped by Laser Diodes. *IEEE J. Sel. Top. Quantum Electron.* **2018**, *24*, 1–10. [[CrossRef](#)]
- Supradeepa, V.R.; Feng, Y.; Nicholson, J.W. Raman fiber lasers. *J. Opt.* **2017**, *19*, 023001. [[CrossRef](#)]
- Terry, N.B.; Alley, T.G.; Russell, T.H. An explanation of SRS beam cleanup in graded-index fibers and the absence of SRS beam cleanup in step-index fibers. *Opt. Express* **2007**, *15*, 17509–17519. [[CrossRef](#)] [[PubMed](#)]
- Kuznetsov, A.G.; Kablukov, S.I.; Podivilov, E.V.; Babin, S.A. Brightness enhancement and beam profiles in an LD-pumped graded-index fiber Raman laser. *OSA Contin.* **2021**, *4*, 1034–1040. [[CrossRef](#)]
- Evmenova, E.A.; Kuznetsov, A.G.; Nemov, I.N.; Wolf, A.A.; Dostovalov, A.V.; Kablukov, S.I.; Babin, S.A. 2nd-order random lasing in a multimode diode-pumped graded-index fiber. *Sci. Rep.* **2018**, *8*, 17495. [[CrossRef](#)]
- Kuznetsov, A.G.; Nemov, I.N.; Wolf, A.A.; Evmenova, E.A.; Kablukov, S.I.; Babin, S.A. Cascaded Generation in Multimode Diode-Pumped Graded-Index Fiber Raman Lasers. *Photonics* **2021**, *8*, 447. [[CrossRef](#)]
- Chen, Y.; Fan, C.; Yao, T.; Xiao, H.; Leng, J.; Zhou, P.; Nemov, I.N.; Kuznetsov, A.G.; Babin, S.A. Brightness enhancement in random Raman fiber laser based on a graded-index fiber with high-power multimode pumping. *Opt. Lett.* **2021**, *46*, 1185–1188. [[CrossRef](#)]
- Kuznetsov, A.G.; Wolf, A.A.; Munkueva, Z.; Babin, S.A. Random lasing in multimode diode-pumped graded-index fiber based on artificial Rayleigh scattering in fs-inscribed random structure. *Proc. SPIE* **2022**, *12310*, 1231018.
- Gagné, M.; Kashyap, R. Demonstration of a 3 mW threshold Er-doped random fiber laser based on a unique fiber Bragg grating. *Opt. Express* **2009**, *17*, 19067–19074. [[CrossRef](#)]
- Lizárraga, N.; Puente, N.P.; Chaikina, E.I.; Leskova, T.A.; Mendez, E.R. Single-mode Er-doped fiber random laser with distributed Bragg grating feedback. *Opt. Express* **2009**, *17*, 395–404. [[CrossRef](#)] [[PubMed](#)]
- Gagné, M.; Kashyap, R. Random fiber Bragg grating Raman fiber laser. *Opt. Lett.* **2014**, *39*, 2755–2758. [[CrossRef](#)] [[PubMed](#)]
- Abdullina, S.R.; Skvortsov, M.I.; Vlasov, A.A.; Podivilov, E.V.; Babin, S.A. Coherent Raman lasing in a short polarization-maintaining fiber with a random fiber Bragg grating array. *Laser Phys. Lett.* **2019**, *16*, 105001. [[CrossRef](#)]

24. Dostovalov, A.V.; Wolf, A.A.; Skvortsov, M.I.; Abdullina, S.R.; Kuznetsov, A.G.; Kablukov, S.I.; Babin, S.A. Femto-second-pulse inscribed FBGs for mode selection in multimode fiber lasers. *Opt. Fiber Technol.* **2019**, *52*, 101988. [[CrossRef](#)]
25. Babin, S.A.; Kuznetsov, A.G.; Sidelnikov, O.S.; Wolf, A.A.; Nemov, I.N.; Kablukov, S.I.; Podivilov, E.V.; Fedoruk, M.P.; Wabnitz, S. Spatio-spectral beam control in multimode diode-pumped Raman fibre lasers via intracavity filtering and Kerr cleaning. *Sci. Rep.* **2021**, *11*, 21994. [[CrossRef](#)] [[PubMed](#)]
26. Volyar, A.V.; Egorov, Y.A. Super pulses of orbital angular momentum in fractional-order spiroid vortex beams. *Opt. Lett.* **2018**, *43*, 74–77. [[CrossRef](#)]
27. Kuznetsov, A.G.; Evmenova, E.A.; Dontsova, E.I.; Kablukov, S.I.; Babin, S.A. Frequency doubling of multimode diode-pumped GRIN-fiber Raman lasers. *Opt. Express* **2019**, *27*, 34760–34768. [[CrossRef](#)]

Disclaimer/Publisher’s Note: The statements, opinions and data contained in all publications are solely those of the individual author(s) and contributor(s) and not of MDPI and/or the editor(s). MDPI and/or the editor(s) disclaim responsibility for any injury to people or property resulting from any ideas, methods, instructions or products referred to in the content.